Journal of ELECTRONIC MATERIALS
https://doi.org/10.1007/s11664-019-07059-z

Increased Degradation Capacity of Methylene Blue Dye Using Mg-doped ZnO Nanoparticles Decorated by Ag^0 Nanoparticles

C.H.R. PAULA,[1] N.F. ANDRADE NETO,[1,2] L.M.P. GARCIA,[1] R.M. NASCIMENTO,[1] C.A. PASKOCIMAS,[1] M.R.D. BOMIO,[1] and F.V. MOTTA[1]

1.—LSQM – Laboratory of Chemical Synthesis of Materials – Department of Materials Engineering, Federal University of Rio Grande do Norte – UFRN, P.O. Box 1524, Natal, RN, Brazil. 2.—e-mail: nfandraden@gmail.com

Photocatalytic activity has been widely used for the treatment of organic effluents, mainly those generated by textile industries. Zinc oxide is widely investigated for this application due to its low cost, non-toxicity and high efficiency. In this work, the photocatalytic properties of ZnO:*x*Mg (*x* = 1 mol.%, 2 mol.%, 4 mol.% and 8 mol.%) decorated with Ag^0 were investigated against methylene blue dye (MB). Initially, the nanostructures of ZnO:*x*Mg were produced by the microwave-assisted hydrothermal method, and the nanoparticles of Ag^0 were deposited by ultraviolet (UV) photoreduction. The structural characteristics of the powders were determined by x-ray diffraction, the morphologies were investigated by field emission scanning electron microscopy (FE-SEM) and the optical absorbance of the photocatalysts was characterized by the diffuse reflectance spectra [UV–visible light (UV–Vis)]. The photocatalytic properties were estimated by degradation of MB, and the capacity for reuse of the powders was estimated by application in three consecutive cycles. Undoped ZnO powders reduced 84% of MB concentration, while the ZnO:8%Mg sample reduced 97% of it, indicating that doping with Mg^{2+} is efficient in increasing the degradation capacity of ZnO against MB degradation. The deposition of metallic silver nanoparticles on the ZnO surface considerably increases the photocatalytic efficiency, in which after 18 min, the 8%Mg sample completely degraded the MB. The reuse tests showed that the powders maintain their photocatalytic activity after three cycles and can be used for such application without generating secondary residues.

Key words: ZnO:*x*Mg, hydrothermal method, Ag^0 photoreduction, photocatalytic reuse

INTRODUCTION

Dyes are organic compounds, chemically stable and absorb large amounts of light. When dyes are discarded without proper treatment, they generate negative changes in the environment.[1–4] Heterogeneous photocatalysis is the most efficient method for degradation of organic dyes, in which conventional methods such as decanting and filtration are not effective.[5] Photocatalytic technology is also widely used because it is a simple oxidation process, based on the light absorption of semiconductors, which act as catalysts.[6–9]

Several materials are currently used in this field of research, such as GdS, CuO, TiO_2 and ZnO.[10,11] Zinc oxide (ZnO) is a promising candidate for environmental applications because it is easy to obtain and has a strong oxidizing capacity; besides,

(Received December 1, 2018; accepted February 9, 2019)

Published online: 23 February 2019

it does not generate risks to human health and environmental impacts.[12–16] The properties of ZnO can be improved by various treatments, such as doping and decoration.[17] Cationic substitution acts positively on the photocatalytic activity due to the possibility of intermediate levels in the prohibited band and the formation of oxygen vacancies that inhibit the recombination of e^-/h^+.[18] Doping with Mg alters the ZnO lattice by forming oxygen/zinc adsorbed on its surface.[19–21]

Another treatment used to optimize the photocatalytic activity is decoration.[22] Decoration with noble metals favors surface plasmon resonance (SPR), where Ag, Au and Pt are normally used,[23] bringing several beneficial effects, since it increases the absorption of visible light and the excitation of carriers of energetic charge.[24] This results in increased redox reactions and higher rate of generation of reactive oxygen species in order to obtain a better separation of charge.[24–26]

In this work, the photocatalytic properties of ZnO:*x*Mg powders (x = 0 mol.%, 1 mol.%, 2 mol.%, 4 mol.% and 8 mol.%) decorated with Ag^0 were investigated by the degradation of the methylene blue dye (MB) under ultraviolet (UV) radiation. The generation of secondary residues is a serious problem in the use of particulates in photocatalytic processes; in order to reduce them, the reuse capacity of the ZnO powders was tested by performing three cycles.

MATERIALS AND METHODS

Synthesis of ZnO:xMg/Ag Nanoparticles

Magnesium nitrate (Sigma-Aldrich, 99%), silver nitrate (Strem Chemicals, 99.9%), sodium hydroxide (Synth, 98%) and deionized water were used to obtain ZnO:*x*Mg/Ag powders.

Initially, zinc nitrate was dissolved in deionized water. Magnesium nitrate, respecting the molar ratios of 1%, 2%, 4% and 8%, was added to the zinc nitrate solution. NaOH was used to set the pH to 10. Subsequently, the solution was brought to the hydrothermal reactor, where it was heated at 140°C by microwave radiation (2.45 GHz and a maximum power of 800 W) and was kept for 15 min. After the synthesis, ZnO:*x*Mg powders were cooled to room temperature, centrifuged and dried at 100°C for 24 h. The ZnO:*x*Mg/Ag nanostructures were obtained using 30 wt.% Ag. A solution containing the powders of ZnO:*x*Mg, distilled water and silver nitrate were kept under stirring and irradiated under UVC light (OSRAM, 15 W, 254 nm) for 1 h for the photoreduction of Ag^0. Finally, the product was filtered, washed and dried at 100°C for 24 h.

Characterization

The phases obtained for ZnO:*x*Mg/Ag powders were investigated using a Shimadzu diffractometer (XRD-6000) with CuKα radiation (1.5418 Å). In order to better verify the changes promoted by doping, refinement was performed using the General Structure Analysis System (GSAS) program with graphic interface EXPGUI.[27] Field emission scanning electron microscopy (FE-SEM) was used to observe the morphology. UV–Vis spectroscopy was performed on Shimadzu (UV-2550) equipment, with a wavelength range of 200–900 nm and programmed for the diffuse reflectance mode. Based on these results, the optical gap band (Egap) energy of these materials was determined using the Wood and Tauc Equation.[28]

Photocatalytic Activities

The photocatalytic properties of the powders were tested against MB of molecular formula [$C_{16}H_{18}ClN_3S$] (Mallinckrodt, with 99.5% purity), under UV–Vis radiation. About 0.05 g of ZnO powders were placed in a beaker containing 50 mL of MB (1.10^{-5} mol L^{-1}) and kept under constant stirring, illuminated by six UVC lamps (OSRAM, 15 W, with maximum intensity of 254 nm = 4.9 eV). At intervals of 10 min for ZnO:*x*Mg samples and intervals of 3 min for ZnO:*x*Mg/Ag samples, 2 mL of aliquot was collected and the absorbance spectrum variation was analyzed using a Shimadzu spectrometer (model UV-2600). By these values, the dye concentration variation was determined according to test time. After the first photocatalytic test, the powder was washed and dried in air, where after drying, it was again contacted with 50 mL of MB of concentration 10^{-5} mol L^{-1}, to carry out the subsequent cycle. This reuse process was repeated two times, totaling three test cycles.

RESULTS AND DISCUSSION

Figure 1a shows the XRD spectrum of ZnO:*x*Mg (with x = 1 mol.%, 2 mol.%, 4 mol.% and 8 mol.%). The XRD peaks were indexed according to JCPDS card no. 89-511. The peaks 2θ = 31.77°, 34.42°, 36.25°, 47.54°, 56.59°, 62.86°, 66.37°, 67.95°, 69.08°, 72.57° and 76.96° correspond to the characteristic planes (100), (002), (101), (102), (110), (103), (200), (112), (201), (004) and (202) referring to the hexagonal structure of ZnO.[29] No secondary peak was observed, indicating that the Mg^{2+} atoms were well-incorporated into the ZnO. Due to the same valence and proximity of the ionic rays of Zn^{2+} and Mg^{2+}, displacement of the characteristic peaks occurred.[30] Figure 1b shows the XRD spectra of ZnO:xMg decorated with Ag^0. Peaks for Ag^0 were indexed according to JCPDS card no. 87-720. The peaks 2θ = 38.11°, 44.30° and 64.44° correspond to the planes (111), (200) and (220) Ag^0. The impregnation of silver in the metallic form is possible due to the lower oxidation potential of Ag^0.

Rietveld refinement was used to analyze possible differences in the structural arrangements induced by the addition of Mg^{2+} in the ZnO lattice.[31] The

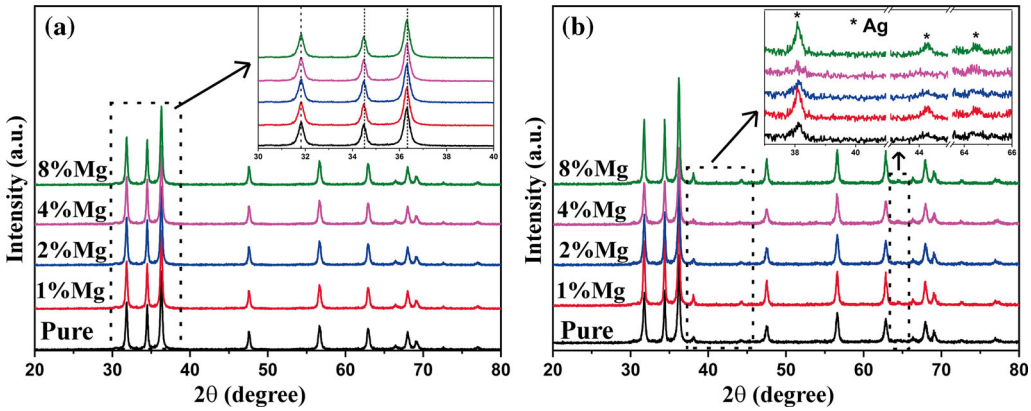

Fig. 1. Diffractograms for the (a) ZnO:*x*Mg and (b) ZnO:*x*Mg/Ag samples.

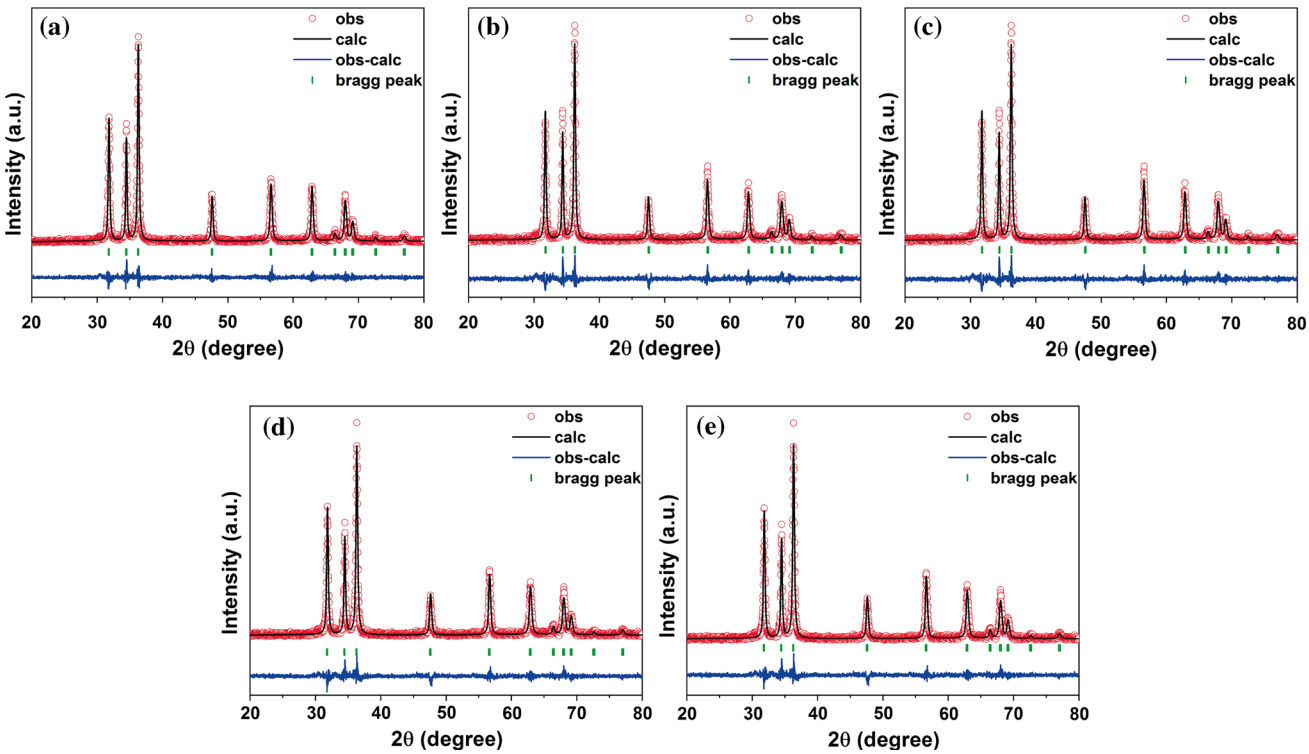

Fig. 2. Rietveld refinement for the (a) ZnO, (b) ZnO:1%Mg, (c) ZnO:2%Mg, (d) ZnO:4%Mg and (e) ZnO:8%Mg samples.

Table I. Structural parameters of the Rietveld refinement for pure and Mg-doped ZnO samples

Sample	ZnO	1%Mg	2%Mg	4%Mg	8%Mg
a (Å)	3.25187	3.25102	3.25102	3.25087	3.25085
c (Å)	5.20817	5.20919	5.20920	5.20900	5.20899
Cell volume (Å^3)	55.0746	55.0566	55.0567	55.0495	55.0487
Crystallite size (nm)	27.70	27.10	26.90	24.57	24.21
Microstrain ($\times 10^3$)	2.6375	2.6219	2.6195	2.3109	1.1016
χ^2	1.254	1.312	1.314	1.346	1.344
R_{wp}	0.2005	0.1978	0.1979	0.2100	0.2098
R_p	0.1356	0.1430	0.1433	0.1443	0.1434
Occ					
Zn^{2+}	1	0.9902	0.9801	0.9606	0.9109
Mg^{2+}	0	0.0098	0.0199	0.0394	0.0891

GSAS program with the EXPGUI graphic interface was used to perform the refinement.[27] JCPDS card no. 89-511 was also used for the refinement. The parameters used in refining were: scale factor and phase fraction; background, which was modeled using a displaced Chebyshev polynomial function; peak shape, which was modeled using the Thomson–Cox–Hastings pseudo-Voigt function; change in lattice constants; fractional atomic coordinates; and isotropic thermal parameters. The results of the Rietveld refinement are shown in Fig. 2 and Table I.

By the small difference obtained between the observed (obs) and theoretically calculated (calc) curves, it is concluded that the diffractogram patterns of the samples are well adapted to JCPDS card no. 89-511. In addition, the reliability parameters χ^2, R_{wp} and R_p exhibit low values, indicating good quality of structural refinements and numerical results. These results confirm that the samples are isostructural, the crystals being well adapted to the cubic structure and spatial group P63mc (no. 186). The values obtained from the occupation of the Zn^{2+} and Mg^{2+} cations in the unit cell are close to the synthesis stoichiometric value, confirming that the doping was successfully performed.

According to Table I, ZnO crystallite size decreases with increasing concentration of Mg^{2+}. This occurs because during the crystal growth, the Mg^{2+} atoms are located near the boundary of the ZnO crystals, reducing their diffusion rate and growth.[32] In addition, the Mg^{2+} (0.78 Å) has a lower ionic radius than Zn^{2+} (0.83 Å). The increase in the amount of the dopant causes more defects in the crystal lattice of ZnO, obtaining smaller sizes of crystallite. This behavior is in accordance with Vergard's law,[33,34] in which for solid metal solutions the unit cell dimensions tend to decrease with an increasing dopant concentration.

The effects induced by doping with Mg on the morphology of ZnO nanoparticles were examined

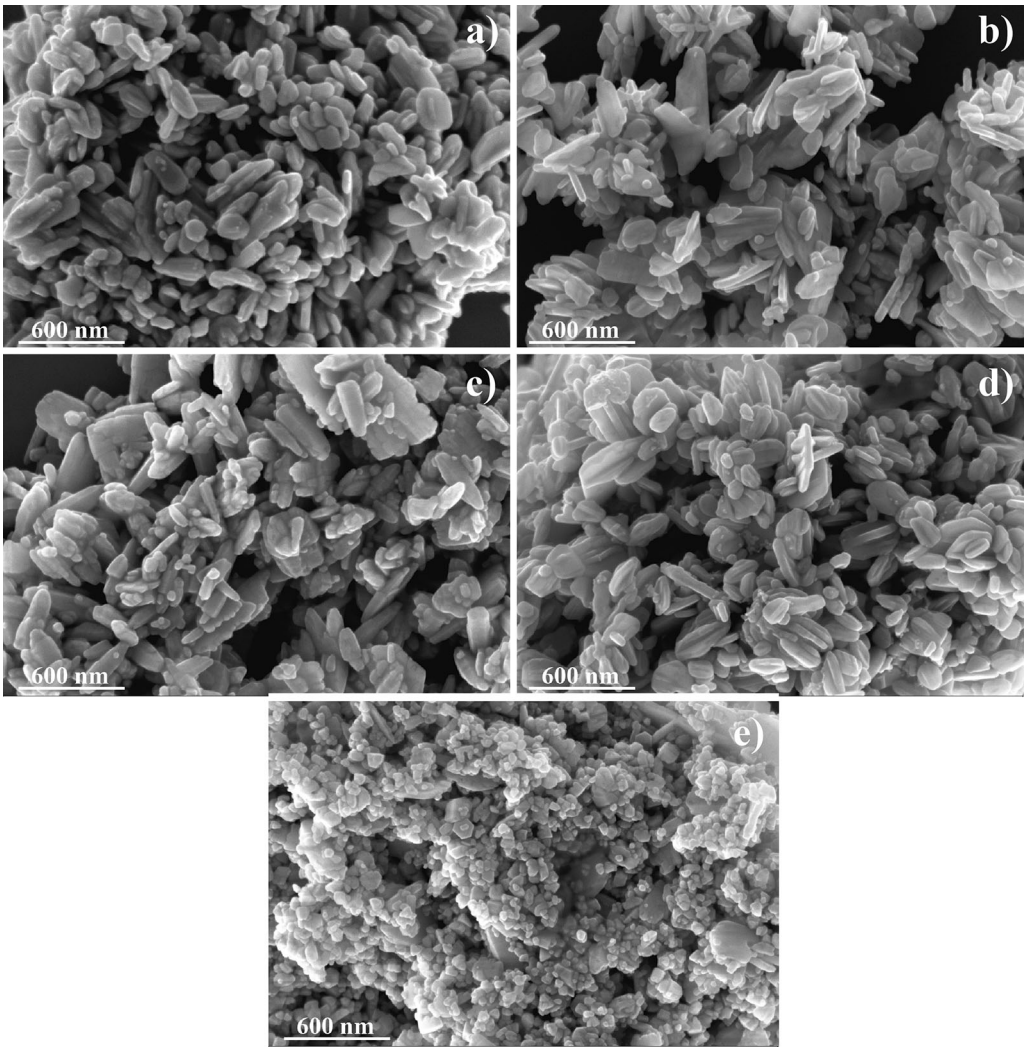

Fig. 3. FE-SEM micrographs of the (a) ZnO, (b) ZnO:1%Mg, (c) ZnO:2%Mg, (d) ZnO:4%Mg and (e) ZnO:8%Mg samples.

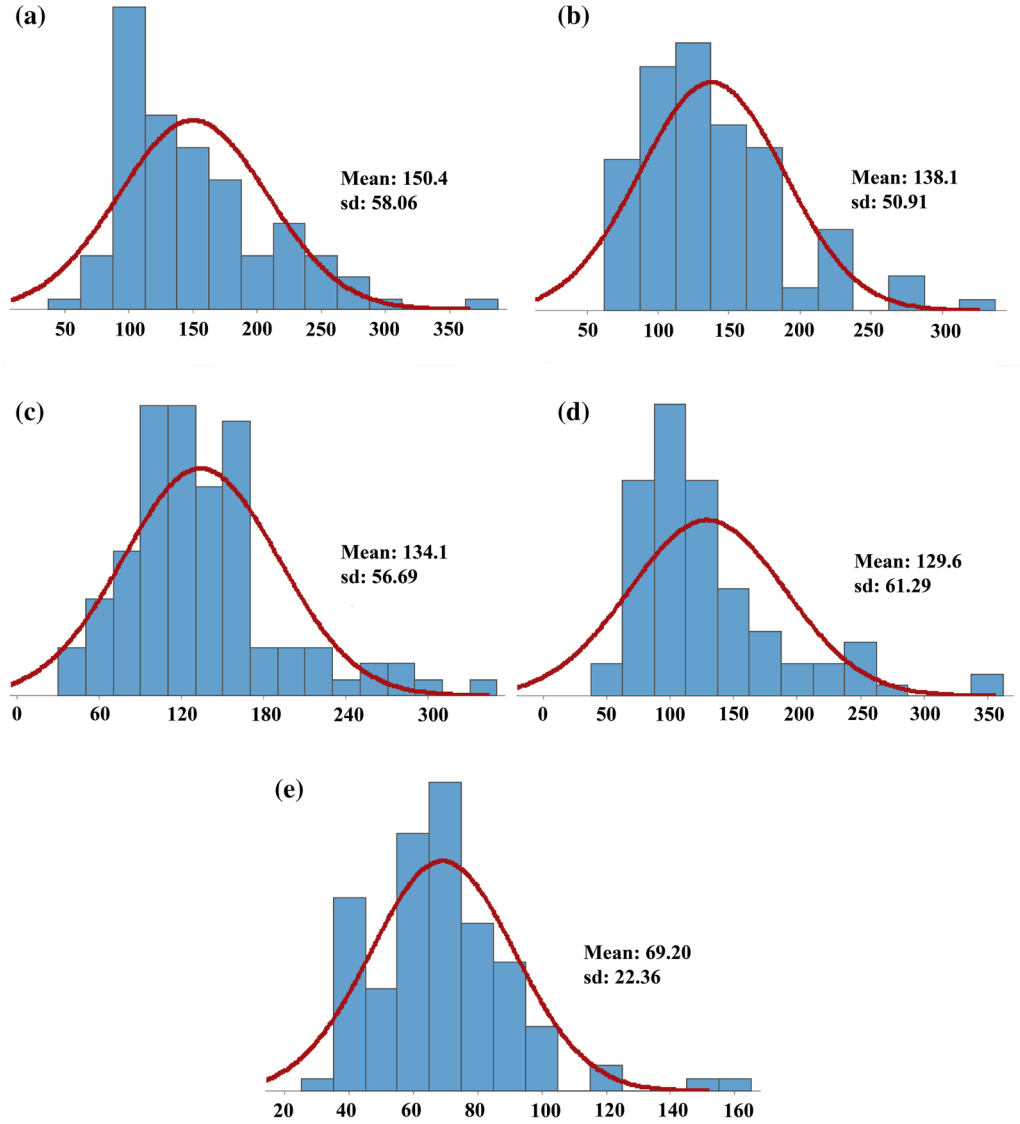

Fig. 4. Histogram of nanoparticle diameters of (a) ZnO, (b) ZnO:1%Mg, (c) ZnO:2%Mg, (d) ZnO:4%Mg and (e) ZnO:8%Mg.

using FE-SEM. Figure 3 shows the morphology of ZnO:*x*Mg nanoparticles. According to Fig. 3, the nanoparticles of ZnO:*x*Mg have their morphology changed as the amount of Mg^{2+} increases. The variation in the morphology can be attributed to the effects induced by the magnesium ions, which have their growth rate altered because they are located in the limits of the ZnO crystals.[32] The reactivity of an element increases as its electronegativity decreases;[35,36] as the electronegativity of Mg (1.31) is less than Zn (1.65), Mg is chemically more reactive. To better observe the influence of Mg on the particle size of ZnO, particle size distributions based on the Gaussian function were assembled, as shown in Fig. 4. Through the data obtained in Fig. 4, the average size of the nanoparticles varies between 150.40 nm and 69.20 nm for the ZnO and ZnO:8%Mg samples, respectively.

To obtain more information about doping with Mg, EDX elemental analysis was performed. Figure 5a and b shows the morphology of ZnO/Ag and ZnO:8%Mg/Ag heterostructures, respectively. The EDX elemental analysis of these heterostructures is observed in Figs. 5c and d. Through the EDX spectra, the formation of Ag^0 is confirmed by the peak appearance around 2.98 keV, referring to the transition Lα1. Confirmation of the doping is evidenced by the spectrum shown in Fig. 5d, where the peak at 1.25 keV is a characteristic of the Mg-kα transition. The peak not shown in Fig. 5 refers to the silicon substrate (Si-kα). EDX spectra confirm the formation of ZnO:8%Mg/Ag heterostructures. According to Fig. 5a and b, decoration with Ag^0 by photodeposition does not alter the morphology of ZnO nanoparticles. The photodeposition of Ag^0 forms fine and dispersed precipitates.

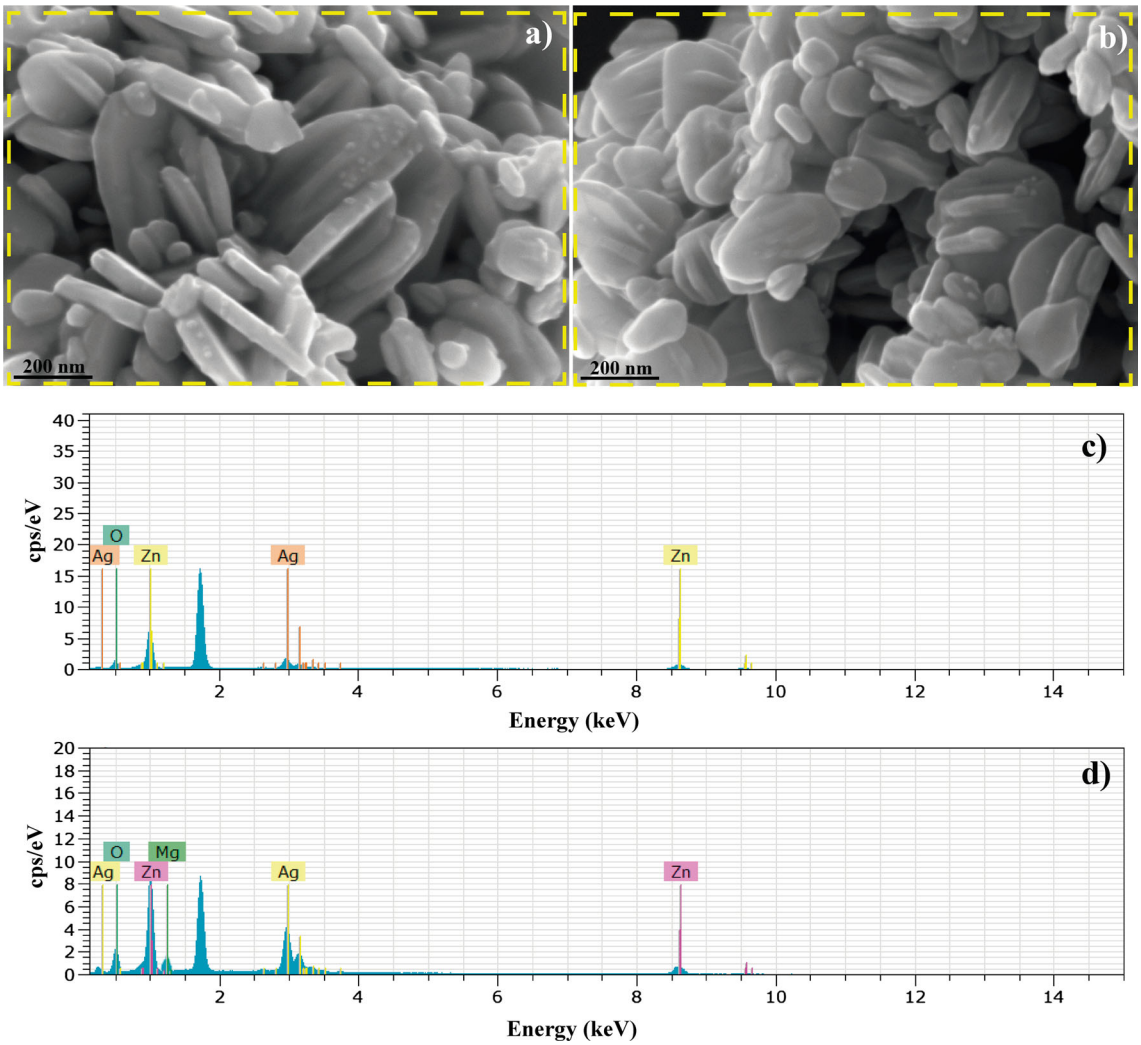

Fig. 5. FE-SEM micrographs and EDX of the (a, c) ZnO/Ag and (b, d) ZnO:8%Mg/Ag samples.

To obtain gap energy (Egap), the reflectance data were converted to absorbance and the absorbance versus photon energy curve was plotted. By the Wood and Tauc method,[28] the extrapolation of this curve gives us the approximate optical Egap value of the powders. Figure 6 shows the absorption spectra in the UV–Visible region for ZnO:*x*Mg powders. The calculated Egap varied from 3.22 eV to 3.24 eV, values that are in agreement with those found in the literature.[37–41] Gupta et al.[42] obtained Egap values varying between 3.23 and 3.18 for samples of iron-doped ZnO, where the reduction of Egap occurred as the concentration of Fe increases. The major changes in the value of the optical gap energy (Egap) can be correlated with the reduction or creation of structural defects or states located within the prohibited area, which may decrease or increase intermediate levels of energy.[43]

According to Wang et al.,[15] ZnO is a type of semiconductor enriched with lattice defects, such as zinc vacancies (VZn), interstitial zinc (Zni), oxygen vacuums (VO) and interstitial oxygen (Oi). Similarly, dopants may also introduce defects in the host ZnO.[44] Additionally, the photocatalytic efficiency of ZnO can be improved by doping with Mg, because in addition to changing the ZnO lattice, it forms oxygen/zinc adsorbed on its surface.[21]

The photocatalytic activity of the ZnO:*x*Mg and ZnO:*x*Mg/Ag powders was evaluated by the degradation of MB when illuminated by UV radiation. Figure 7a shows the photocatalytic activity of ZnO:*x*Mg and Fig. 7b shows the photocatalytic activity of ZnO:*x*Mg/Ag. The photocatalytic process can be described by a first-order kinetic model with respect to the absorbance of MB.[45] The curves formed by the ln C/Co versus test time are shown in Fig. 7c and d for samples without and with decorated Ag^0, respectively. The values of the constant k ($\times 10^{-2}$ min^{-1}) are shown in Fig. 7.

As can be seen in Fig. 7a, the addition of Mg^{2+} provides an increase in photocatalytic activity. As previously seen, the substitution of Zn^{2+} ions for Mg^{2+} provides smaller nanoparticles, thus increasing the interaction between the nanoparticles and

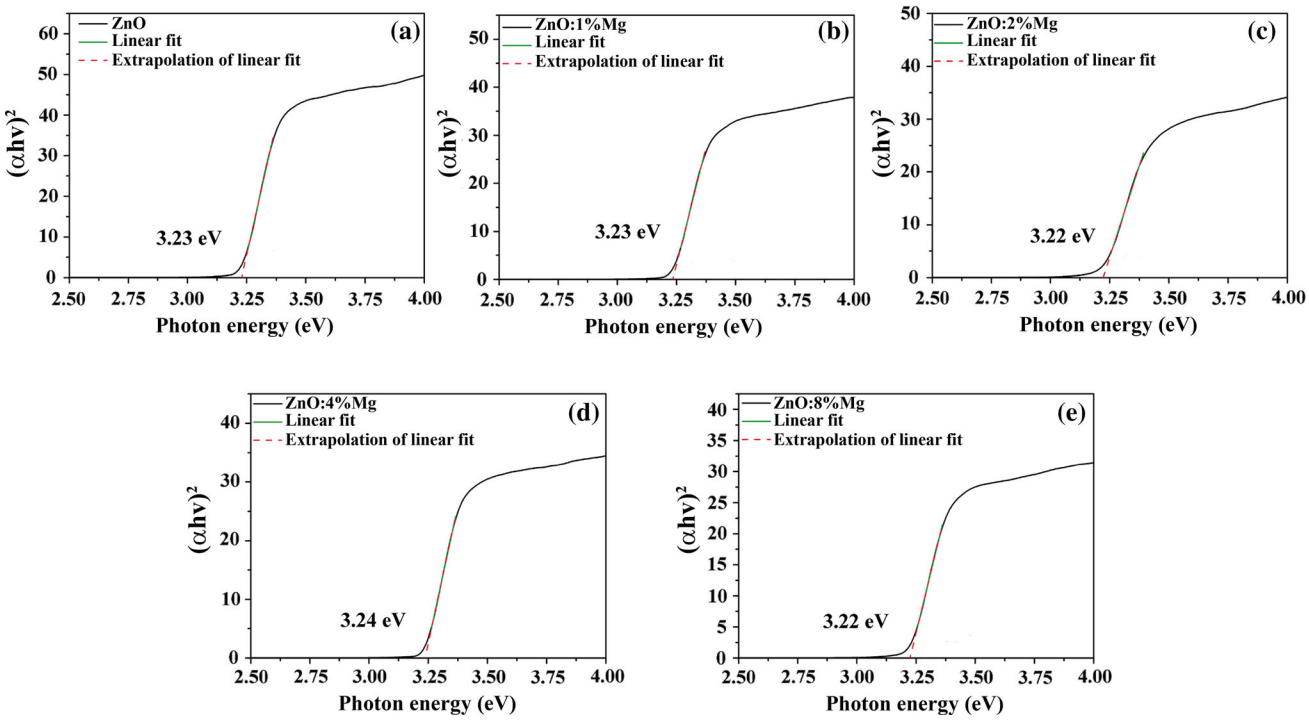

Fig. 6. Absorption spectra in the UV–visible region by extrapolating the linear region of the curve according to the Wood and Tauc method for samples of (a) ZnO, (b) ZnO:1%Mg, (c) ZnO:2%Mg, (d) ZnO:4%Mg and (e) ZnO:8%Mg.

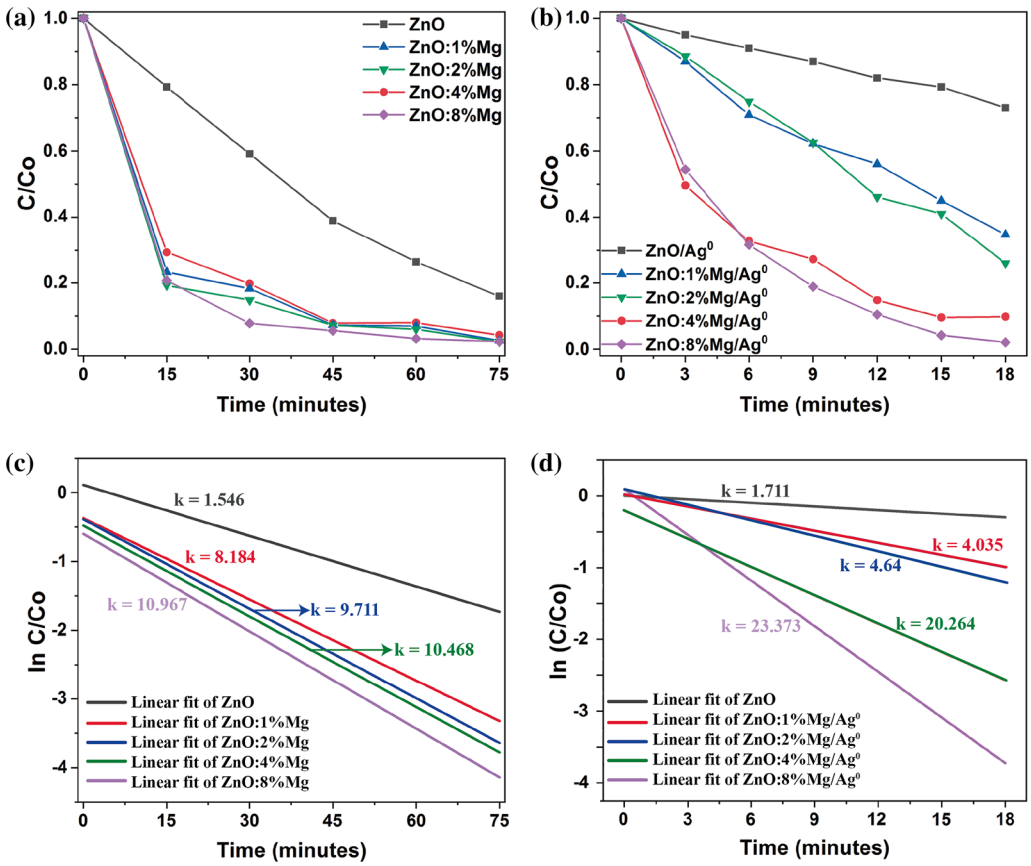

Fig. 7. Variation of methylene blue dye concentration (initial concentration of 1.10^{-5} mol L^{-1}) by time of assay using 0.05 g of catalyst and 50 mL of methylene blue dye and model for obtaining the first-order kinetic constant for (a, c) ZnO:*x*Mg and (b, d) ZnO:*x*Mg/Ag samples (Color figure online).

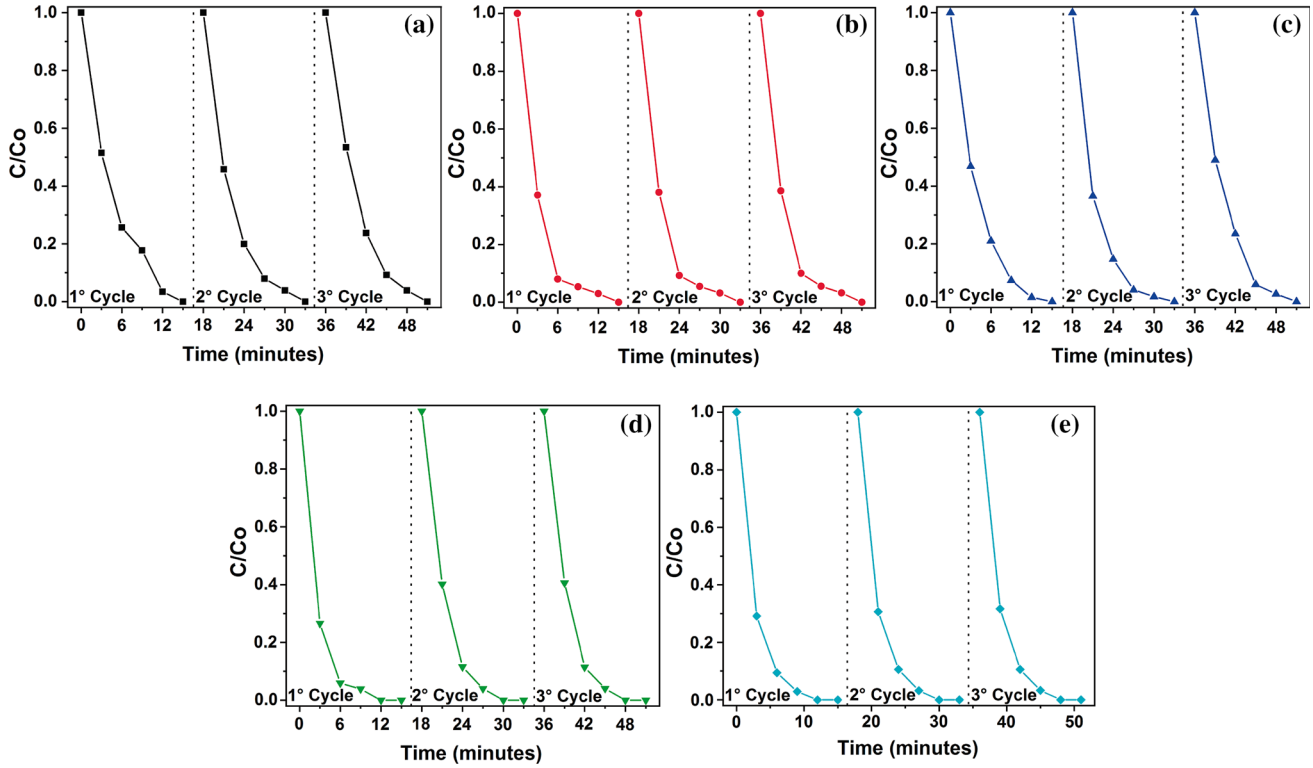

Fig. 8. Photocatalytic reuse maintaining the ratio of catalyst/dye (1 g/1 L) for (a) ZnO/Ag, (b) ZnO:1%Mg/Ag, (c) ZnO:2%Mg/Ag, (d) ZnO:4%Mg/Ag and (e) ZnO:8%Mg/Ag samples.

the dye molecules.[46] Moreover, the defects generated by this substitution acted to suppress recombination of the electron/hole pairs.[11,21]

Figure 7b shows that the silver decoration significantly increases the photocatalytic efficiency of the ZnO powders, where the ZnO:8%Mg/Ag sample completely degraded the MB after 18 min. According to Sohrabnezhad et al.,[24] this result occurs due to surface plasmon resonance (SPR), which causes increased redox reactions and higher rates of generation of reactive oxygen species. Additionally, the heterojunction formed between ZnO and Ag^0 nanoparticles acts in order to increase the separation of the charge carriers providing species that are more reactive to act in the photocatalysis.[22,25,47]

The ZnO:*x*Mg/Ag heterostructures proved to be very efficient in the degradation of MB, as shown in Fig. 7. However, photocatalysts in powder form after the photocatalytic process require treatment to be discarded.[48] An alternative to minimize this problem is the possibility of reusing the powders. The possibility of reusing the powders, in cycles in a row, without needing specific treatment, makes them good candidates for large-scale applications. In order to analyze the capacity of the ZnO:*x*Mg/Ag powders to be reused, they were submitted to three cycles, without accomplishment of thermal treatment. Figure 8 shows the reuse curves for ZnO:*x*Mg/Ag powders.

The estimation of the kinetic constant is extremely important, since it provides quantitative data about the photocatalytic process.[49,50] For the best comparative effect on the samples with and without Ag^0, the kinetic constant was estimated for the same test time, with 18 min. The samples with 4 and 8% Mg presented the highest kinetic constants, being 20.264 and 23.373, respectively. These values coincide with those presented by the C/Co curves, presenting the best photocatalytic results against the MB. The reuse capacity of the powders should be evaluated by two methods: ease of reuse and maintenance of their photocatalytic activity with the reuse sequence.[51,52] Figure 8 shows that the ZnO:*x*Mg/Ag compounds maintain their photocatalytic efficiency even after the third cycle, indicating that the powders exhibit high chemical stability and can be reused sequentially.

CONCLUSION

Nanoparticles of ZnO:*x*Mg with hexagonal Wurtizite polycrystalline structure were easily obtained by the microwave-assisted hydrothermal method at 140°C for 15 min without forming secondary phases. Photoreduction by UVC radiation was efficient to obtain Ag^0 on the surface of ZnO:*x*Mg nanoparticles without any chemical interaction. The addition of Mg^{2+} provides the reduction in the particle size of ZnO. The decrease in the size of the nanoparticles, together with the defects generated in the crystalline lattice of ZnO from doping with Mg^{2+}, optimizes the photocatalytic activity.

This photocatalytic performance was potentiated with the decoration with Ag^0 due to SPR. The easy attainment of the ZnO:*x*Mg/Ag heterostructures parallel to the high photocatalytic potential and reusability make this material promising for applications in the treatment of textile effluents.

ACKNOWLEDGMENTS

This study was partially financed in part by the Coordenação de Aperfeiçoamento de Pessoal de Nível Superior—Brasil (CAPES/PROCAD)—finance code 2013/2998/2014, and the authors are thankful for the financial support of the Brazilian Research Financing Institution: CNPq No. 307546/2014.

REFERENCES

1. B. Bohnenkamp, J.-H. Linnemann, I.J. Junger, E. Schwenzfeier-Hellkamp, and A. Ehrmann, *Optik* 168, 282 (2018).
2. D. Shu, K. Fang, X. Liu, Y. Cai, X. Zhang, and J. Zhang, *J. Clean. Prod.* 196, 935 (2018).
3. A. Gao, H. Liu, H. Zhang, F. Danna, A. Hou, and K. Xie, *J. Clean. Prod.* 200, 48 (2018).
4. X. Huan-Yan, B. Li, T.-N. Shi, Y. Wang, and S. Komarneni, *J. Colloid Interface Sci.* 532, 161 (2018).
5. C. Byrne, G. Subramanian, and S.C. Pillai, *J. Environ. Chem. Eng.* 6, 3531 (2018).
6. S.T. Kochuveedu, *J. Nanomater.* 2016, 12 (2016).
7. T. Hisatomi, J. Kubota, and K. Domen, *Chem. Soc. Rev.* 43, 7520 (2014).
8. M.-Q. Yang, and X. Yi-Jun, *Nanoscale Horizons* 1, 185 (2016).
9. M.-Q. Yang, C. Han, and X. Yi-Jun, *J. Phys. Chem. C* 119, 27234 (2015).
10. F. Zhang, X.-Q. Kong, Q. Li, T.-T. Sun, C. Chai, W. Shen, Z.-Y. Hong, X.-W. He, W.-Y. Li, and Y.-K. Zhang, *Talanta* 148, 108 (2016).
11. N.F. Andrade Neto, E. Longo, K.N. Matsui, C.A. Paskocimas, M.R.D. Bomio, and F.V. Motta, *Plasmonics* 14, 79 (2019).
12. A. Rosli, Z. Awang, S.S. Shariffudin, and S.H. Herman: *Annealing Temperature Dependence of ZnO Nanostructures Grown by Facile Chemical Bath Deposition for EGFET pH Sensors*. (2018).
13. L.G.A. Carvalho, L.A. Rocha, J.M.M. Buarque, R.R. Gonçalves, C.S. Nascimento Jr, M.A. Schiavon, S.J.L. Ribeiro, and J.L. Ferrari, *J. Lumin.* 159, 223 (2015).
14. L. Schmidt-Mende, and J.L. MacManus-Driscoll, *Mater. Today* 10, 40 (2007).
15. Z.L. Wang, *Mater. Today* 7, 26 (2004).
16. M.A. Hernández-Carrillo, R. Torres-Ricárdez, M.F. García-Mendoza, E. Ramírez-Morales, L. Rojas-Blanco, L.L. Díaz-Flores, G.E. Sepúlveda-Palacios, F. Paraguay-Delgado, and G. Pérez-Hernández, *Catal. Today* (2018). https://doi.org/10.1016/j.cattod.2018.04.060.
17. M.M. Ovhal, A. Santhosh Kumar, P. Khullar, M. Kumar, and A.C. Abhyankar, *Mater. Chem. Phys.* 195, 58 (2017).
18. A. Das, P.G. Roy, S. Sen, and A. Bhattacharyya, *Thin Solid Films* 662, 54 (2018).
19. Y. Zhao, L. Liu, T. Cui, G. Tong, and W. Wenhua, *Appl. Surf. Sci.* 412, 58 (2017).
20. W. Xiao, W. Zhou, Y. Zhang, L. Tian, H. Liu, and P. Yong, *J. Nanomater.* 2016, 11 (2016).
21. P.K. Labhane, S.H. Sonawane, G.H. Sonawane, S.P. Patil, and V.R. Huse, *J. Phys. Chem. Solids* 114, 71 (2018).
22. Y. Wang, R. Shi, J. Lin, and Y. Zhu, *Energy Environ. Sci.* 4, 2922 (2011).
23. Y.-Z. Xing, H.F. Zhang, X.-B. Liu, and Y.-M. Zheng, *Nucl. Phys. A* 957, 135 (2017).
24. Sh Sohrabnezhad, and A. Seifi, *Appl. Surf. Sci.* 386, 33 (2016).
25. W.L. Ong, S. Natarajan, B. Kloostra, and G.H. HO, *Nanoscale* 5, 5568 (2013).
26. S. Kuriakose, V. Choudhary, B. Satpati, and S. Mohapatra, *Beilstein J. Nanotechnol.* 5, 639 (2014).
27. B. Toby, *J. Appl. Crystallogr.* 34, 210 (2001).
28. D.L. Wood, and J. Tauc, *Phys. Rev. B* 5, 3144 (1972).
29. H. Jiang, X. Zhang, G. Wen, X. Feng, L. Zhang, and Y. Weng, *Chem. Phys. Lett.* 711, 100 (2018).
30. S.A. Ibitoye, and A.A. Afonja, *J. Miner. Mater. Charact. Eng.* 07, 10 (2008).
31. H. Rietveld, *J. Appl. Crystallogr.* 2, 65 (1969).
32. A.N. Mallika, A. Ramachandra Reddy, K. Sowri Babu, Ch Sujatha, and K. Venugopal Reddy, *Opt. Mater.* 36, 879 (2014).
33. M.J. McKelvy, R. Sharma, A.V.G. Chizmeshya, R.W. Carpenter, and K. Streib, *Chem. Mater.* 13, 926 (2001).
34. F.V. Motta, A.P.A. Marques, M.S. Li, M.F.C. Abreu, C.A. Paskocimas, M.R.D. Bomio, R.P. Souza, J.A. Varela, and E. Longo, *J. Alloy. Compd.* 553, 338 (2013).
35. Y. Su-Hua, H. Sheng-Yu, and T. Cheng-Hsun, *Jpn. J. Appl. Phys.* 49, 06GJ06 (2010).
36. J. Iqbal, T. Jan, M. Ismail, N. Ahmad, A. Arif, M. Khan, M. Adil, H. Sam ul, and A. Arshad, *Ceram. Int.* 40, 7487 (2014).
37. N.F. Andrade Neto, K.N. Matsui, C.A. Paskocimas, M.R.D. Bomio, and F.V. Motta, *Mater. Sci. Semicond. Process.* 93, 123 (2019).
38. B. Dindar, and A.C. Güler, *Environ. Nanotechnol. Monit. Manag.* 10, 457 (2018).
39. C. Jaramillo-Páez, J.A. Navío, and M.C. Hidalgo, *J. Photochem. Photobiol. A* 356, 112 (2018).
40. L. Liu, Z. Liu, Y. Yang, M. Geng, Y. Zou, M. Babar Shahzad, Y. Dai, and Y. Qi, *Ceram. Int.* 44, 19998 (2018).
41. J. Kaur, K. Gupta, V. Kumar, S. Bansal, and S. Singhal, *Ceram. Int.* 42, 2378 (2016).
42. I. Zammit, V. Vaiano, G. Iervolino, and L. Rizzo, *RSC Adv.* 8, 26124 (2018).
43. Z.M. Gibbs, A. LaLonde, and G. Jeffrey Snyder, *New J. Phys.* 15, 075020 (2013).
44. Y. Wang, J. Piao, L. Yunhao, S. Li, and J. Yi, *Mater. Res. Bull.* 83, 408 (2016).
45. M.M. Momeni, M. Hakimian, and A. Kazempour, *Ceram. Int.* 41, 13692 (2015).
46. N. Neto, P.M. Oliveira, R. Nascimento, C.A. Paskocimas, M.R.D. Bomio, and F.V. Motta, *Ceram Int* 45, 651 (2018).
47. R. Gupta, N.K. Eswar, J.M. Modak, and G. Madras, *Catal. Today* 300, 71 (2018).
48. L.M.P. Garcia, M.T.S. Tavares, N.F. Andrade Neto, R.M. Nascimento, C.A. Paskocimas, E. Longo, M.R.D. Bomio, and F.V. Motta, *J. Mater. Sci. Mater. Electron.* 29, 6530 (2018).
49. W.-K. Wang, J.-J. Chen, M. Gao, Y.-X. Huang, X. Zhang, and Y. Han-Qing, *Appl. Catal. B* 195, 69 (2016).
50. L. Li, Y. Yang, X. Liu, R. Fan, Y. Shi, S. Li, L. Zhang, X. Fan, P. Tang, X. Rui, W. Zhang, Y. Wang, and L. Ma, *Appl. Surf. Sci.* 265, 36 (2013).
51. J. Dantas, E. Leal, D.R. Cornejo, and A.C.F.M. Costa, *Arab. J. Chem.* (2018). https://doi.org/10.1016/j.arabjc.2018.08.012.
52. S. Dehghan, B. Kakavandi, and R.Z. Kalantary, *J. Mol. Liq.* 264, 98 (2018).